Peristaltic pumping of a viscoelastic fluid for large Weissenberg numbers and high occlusion.

Hector D. Ceniceros

Department of Mathematics, University of California Santa Barbara, CA 93106

Jordan E. Fisher

Department of Mathematics, University of California Santa Barbara, CA 93106

Abstract

Peristaltic pumping is a mechanism for transporting fluid prevalently utilized in both biological organisms and human designed systems. The mechanism induces flow in a channel by contracting the channel's walls in a set pattern. Peristaltic pumping of Newtonian fluids is well understood, and recent investigations have begun exploring the nature of peristalsis of non-Newtonian fluids. Here we investigate the particular case of peristalsis of an Oldroyd- B fluid via an Immersed Boundary method. We utilize a new, highly efficient semi-implicit solver for the equations of the flow and the immersed contracting walls which allows us to explore extreme parameter regimes, including those where the polymeric stress is many orders of magnitude larger than previously accessible to numerical experiments. In particular, we consider large Weissenberg numbers and high channel occlusions. A new dynamic behavior is observed with substantial effects on the pumping flow rate, including evidence for a finite-time blow up of the Oldroyd- B equations.

Keywords: Oldroyd-B, peristaltic, Immersed Boundary, semi-implicit method

Email addresses: hdc@math.ucsb.edu (Hector D. Ceniceros), www.math.ucsb.edu/~hdc (Hector D. Ceniceros), jordan@math.ucsb.edu (Jordan E. Fisher)

1. Introduction

Peristalsis is the predominant mechanism of action in a plethora of biological phenomena, from earthworm mobility to gastrointestinal and esophageal transport. Peristalsis is utilized in many mechanical fluid pumps, often because of their ability to effectively transport highly viscous fluids. In both biological and mechanical systems, the fluid internal to the pump may be non-Newtonian. Such is the case for peristalsis in the oviduct and uterus where the transported biological fluid is highly complex.

Recent work has begun the investigation of peristalsis of an Oldroyd B (OB) fluid [6, 3]. A marked difference has been reported with respect to the Newtonian flow counterpart, particularly the non-linear relationship between mean flow through the pump and the Weissenberg number of the fluid. It has been noted in these works that the polymeric stress of the transported fluid can lead to very strong normal stresses at the interface with the pump. These stresses present a difficult numerical problem. In order to correctly model the structure of the pump wall very stiff forces must be employed, leading to very small time-step constraints. Such numerical constraints (stiffness) are particularly pernicious for explicit Immersed Boundary (IB) methods, as used in [6, 3]. There, the numerical stiffness limited the range of parameters ameanable to investigate. In Section 3, we present a new numerical method coupling a viscoelastic fluid solver to a novel, highly efficient semi-implicit implementation of the IB method, presented in more detail in [1, 2]. The implicit methodology allows us to explore extreme parameter regimes previously out of reach of numerical algorithms. In particular, when the waves of peristalsis have very large amplitude, nearly occluding the channel, the normal stresses on the wall become extremely large. In addition, for very large Weissenberg numbers the transported fluid can develop very strong stresses, even for moderate occlusions. The implicit methodology allows us to robustly probe both of these regimes. Previous work has hinted at interesting behavior as the pump occlusion is increased, including substantial effects on the pump's rate of flow. We probe these effects for substantially larger occlusions than previously possible. In Section 4 we detail new behavior observed, including evidence for a finite-time blow up of the OB equations.

2. The Peristaltic Pump and Viscoelastic Fluid Models

We consider a peristaltic pump immersed in a period 2D domain $\Omega = [0,1]^2$. We model the peristaltic pump as two disconnected sinusoidal curves,

$$\mathbf{X}(t) = \left\{ \left(\xi, \frac{1}{2} + d(\xi, t) \right) \Big| \xi \in [0,1] \right\} \cup \left\{ \left(\xi, \frac{1}{2} - d(\xi, t) \right) \Big| \xi \in [0,1] \right\} \quad (1)$$

where

$$d(x,t) = \frac{\alpha}{2\pi}[1 + \chi \sin 2\pi(\xi - t)]. \quad (2)$$

Both the spatial and temporal period of the pump is fixed at 1. As time progresses the waves of peristalsis move from left to right, forcing the fluid to flow to the right (in aggregate). The parameter χ represents the occlusion ratio of the pump. The value $\chi = 0$ corresponds to a straight channel , with no waves of peristalsis, while $\chi = 1$ correspond to a completely occluded channel, with the peaks of each sinusoidal curve meeting at some point along the horizontal line $y = 1/2$. The parameter α controls the aspect ratio of the channel. For this work we fix $\alpha = 1.5$.

We model the interior and exterior of the valve as one continuous Oldroyd B (OB) incompressible fluid. The interaction between the valve and the fluid is captured via the Immersed Boundary Method. The continuous equations are then

$$Re \left(\frac{\partial \mathbf{u}}{\partial t} + \mathbf{u} \cdot \nabla \mathbf{u} \right) = -\nabla p + \nabla^2 \mathbf{u} + \beta \nabla \cdot \mathbf{S} + \mathbf{f}, \quad (3)$$

$$\nabla \cdot \mathbf{u} = 0, \quad (4)$$

$$\frac{\partial \mathbf{X}}{\partial t} = \mathbf{u}(\mathbf{X}, t), \quad (5)$$

$$\mathbf{S}^{\nabla} = -We^{-1}(\mathbf{S} - \mathbf{I}). \quad (6)$$

Here $\mathbf{f}$ can be seen as a Lagrange multiplier used to enforce the prescribed motion of the peristaltic waves. Due to the no slip boundary condition (5) we can only modulate $\mathbf{X}$ by modifying the fluid velocity $\mathbf{u}$. In practice, we will only enforce the prescribed position of $\mathbf{X}$ approximately by taking $\mathbf{f}$ to be a very stiff force binding the current configuration $\mathbf{X}$ to the desired prescribed position given by (1).

In (3), Re is the Reynolds number which is a measure of the viscous dissipation relative to inertial forces. The dimensionless term β specifies the

strength of the viscoelastic force $\nabla \cdot \mathbf{S}$. Here, $\mathbf{S}$ is the deviatoric part of of the viscoelastic stress tensor and evolves according to the OB constitutive equation, given in (6). $\mathbf{S}^{\nabla}$ denotes the upper convected derivative of $\mathbf{S}$, namely

$$\mathbf{S}^{\nabla} = \frac{d\mathbf{S}}{dt} + \mathbf{u} \cdot \nabla \mathbf{S} - \nabla \mathbf{u} \cdot \mathbf{S} - \mathbf{S} \cdot \nabla \mathbf{u}^T. \tag{7}$$

We is a dimensionless parameter giving the ratio of the relaxation time of the polymeric stress $\mathbf{S}$ against some characteristic time scale of the fluid. We is referred to as the Weissenberg number of the fluid. In the limit as $We \to 0$ the polymeric stress is fixed as the identity tensor $\mathbf{I}$ and the fluid becomes Newtonian. In general the larger the value of We the larger the non-Newtonian effect on the fluid.

Finally, the product βWe is the ratio of the polymeric viscosity to the solvent viscosity. Following Teran, Fauci, Shelly [6] we fix $\beta We = \frac{1}{2}$. As mentioned above, we choose the characteristic length scale to be 1, the width of our fluid domain Ω and the characteristic timescale we also take it to be 1, the period of the peristaltic pump. We fix the Reynolds number of our fluid at $Re = 1$. Throughout this work the only fluid parameter we change is the Weissenberg number We.

3. Methodology

We discretize the peristaltic pump $\mathbf{X}$ as a collection of N_B immersed points $\{\mathbf{X}_j\}$. The position of these points are not directly prescribed, rather we construct an artificial force to approximately constrain the immersed points to their respective positions. For each point $\mathbf{X}_j$ we define $\mathbf{T}_j$ to be the desired target position. We then induce a force $\mathbf{F}$ defined on immersed points given by

$$\mathbf{F} = \sigma(\mathbf{T} - \mathbf{X}). \tag{8}$$

The scalar variable σ is a numerical parameter. In the limit as $\sigma \to \infty$ we exactly constrain $\mathbf{X}$ to the desired configuration. In practice we take σ to be some large value. This can lead to instability in the resulting numerical simulations. We counter this by employing a new semi-implicit methodology as detailed in [1, 2]. With the semi-implicit method we can use values of σ multiple orders of magnitude larger than previously possible. For the large values of We and χ explored in this work we are required to take $\sigma = O(10^6)$ to maintain the structure of the pump. This large stiffness coefficient would

lead to prohibitively small time-steps for previous explicit methods. In our numerical experiments our choice of σ reduces deviations in $\mathbf{X}$ from the target position $\mathbf{T}$ to less than .0005 units, even when the normal polymeric stresses at the boundary rise to values of 1000 and more.

We briefly overview the semi-implicit method here. The method is based on a semi-implicit discretization of the Navier-Stokes equations given by

$$\frac{\mathbf{u}^{n+1}-\mathbf{u}^n}{\Delta t}+\mathbf{u}^n\cdot\nabla\mathbf{u}^n=-\mathbf{D}_h p^{n+1}+L_h\mathbf{u}^{n+1}+\mathbf{f}, \tag{9}$$

$$\mathbf{D}_h\cdot\mathbf{u}^{n+1}=0, \tag{10}$$

$$\frac{\mathbf{X}^{n+1}-\mathbf{X}^n}{\Delta t}=\mathcal{S}_n^*\mathbf{u}^{n+1}. \tag{11}$$

Here a superscript n denotes a numerical approximation taken at the time $n\Delta t$ and Δt is the timestep. The spatial operators $\mathbf{D}_h$ and L_h are the standard, second order approximations to the gradient and the Laplacian, respectively. The convection term $\mathbf{u}^n\cdot\nabla\mathbf{u}^n$ is handled separately via a third-order essentially non-oscillatory (ENO) scheme. The force $\mathbf{F}$ in (8) is defined at the immersed points and can not be directly used in the fluid equations (3)-(6). First we must *spread* the force onto the surrounding Eulerian grid. Likewise in equation (11) the fluid velocity is not given at the immersed points, so we must *interpolate* the fluid velocity. To achieve the spreading and interpolation we define

$$(\mathcal{S}_n G)(\mathbf{x})=\sum_{s\in\mathcal{G}_B} G(s)\delta_h(\mathbf{x}-\mathbf{X}^n(s))h_B, \tag{12}$$

$$(\mathcal{S}_n^* w)(s)=\sum_{\mathbf{x}\in\mathcal{G}_\Omega} w(\mathbf{x})\delta_h(\mathbf{x}-\mathbf{X}^n(s))h^2, \tag{13}$$

known as the spreading and interpolation operators, respectively. Here $\delta_h(\mathbf{x})\equiv d_h(\mathbf{x}_0)d_h(\mathbf{x}_1)$ is an approximation to the two-dimensional Dirac delta distribution and d_h is given by

$$d_h(r)=\begin{cases}\frac{1}{4h}\left(1+\cos(\frac{\pi r}{2h})\right) & \text{if } |r|\le 2h,\\ 0 & \text{otherwise.}\end{cases} \tag{14}$$

We refer to these operators as lagged because the interface configuration $\mathbf{X}^n$ is used instead of the future configuration $\mathbf{X}^{n+1}$.

Utilizing $\mathcal{S}_n$ and $\mathcal{S}_n^*$ we now specify the form of $\mathbf{f}$ in (9).

$$\mathbf{f} = \sigma \mathcal{S}_n(\mathbf{T}^{n+1} - \mathbf{X}^{n+1}) + \beta \mathbf{D}_h \cdot \mathbf{S}^n, \tag{15}$$

encapsulating both the artificial force on the immersed points, as well as the additional force coming from the polymeric stress. We thus consider the polymeric stress fixed as we update the fluid. Once we have an updated fluid velocity $\mathbf{U}^{n+1}$ we will then calculate an updated value for the stress $\mathbf{S}^{n+1}$.

We may formally eliminate $\mathbf{u}^{n+1}$ from the equations (3)-(6), arriving at a *linear* system of the form

$$\mathbf{X}^{n+1} = \sigma \mathcal{M}_n(\mathbf{T}^{n+1} - \mathbf{X}^{n+1}) + \mathbf{b}^n, . \tag{16}$$

We refer to this as the Lagrangian system. $\mathcal{M}_n$ is an operator acting on a force distribution $\mathbf{F}$ and returning the resulting displacement of immersed points due to the induced fluid flow from the spread force $\mathcal{S}_n\mathbf{F}$. Critically, both $\mathcal{M}_n$ and $\mathbf{b}^n$ can be explicitly constructed in an efficient manner, yielding a $2N_B \times 2N_B$ matrix and $2N_B$ vector respectively. We detail this construction in our previous papers [1, 2]. The resulting system can be rewritten as a simple matrix inversion problem

$$(I + \sigma \mathcal{M}_n)\mathbf{X}^{n+1} = \sigma \mathbf{T}^{n+1} + \mathbf{b}^n, . \tag{17}$$

The matrix $I + \sigma\mathcal{M}_n$ is positive-definite and the system (17) can be inverted in a number of ways, the most efficient being multigrid. For the present work conjugate gradient suffices to provide a nearly optimal solver. Once we have solved (17) for the updated configuration $\mathbf{X}^{n+1}$ we may then calculate the updated fluid velocity via (3)-(10).

Finally we must calculate the updated polymeric stress $\mathbf{S}^{n+1}$. Recall the constitutive equation (6) given as $\mathbf{S}^{\nabla} = -We^{-1}(\mathbf{S} - \mathbf{I})$. We discretize this in space as

$$\frac{d\mathbf{S}}{dt} + \mathbf{u}^{n+1} \cdot \nabla \mathbf{S}^n = \mathbf{D}_h \mathbf{u}^{n+1} \cdot \mathbf{S}^n + \mathbf{S}^n \cdot \mathbf{D}_h (\mathbf{u}^{n+1})^T + \frac{1}{We}(\mathbf{I} - \mathbf{S}^n). \tag{18}$$

Here the convective term $\mathbf{u}^{n+1} \cdot \nabla \mathbf{S}^n$ is calculated via the third-order ENO scheme, as with the convection in the momentum equation (9). We further discretize in time via a second-order total variation diminishing (TVD) Runge-Kutta method. If we define the Euler update operator

$$E(\mathbf{S}) = \mathbf{S} + \Delta t \left[\mathbf{D}_h \mathbf{u}^{n+1} \cdot \mathbf{S} + \mathbf{S} \cdot \mathbf{D}_h (\mathbf{u}^{n+1})^T + \frac{1}{We}(\mathbf{I} - \mathbf{S}) - \mathbf{u}^{n+1} \cdot \nabla \mathbf{S} \right], \tag{19}$$

then our Runge-Kutta update is given as $\mathbf{S}^{n+1} = (\mathbf{S}^n + E(E(\mathbf{S}^n)))/2$.

3.1. Summary of algorithm

Given $\mathbf{X}^n$, $\mathbf{u}^n$, $\mathbf{S}^n$ at time $t = n\Delta t$, a complete timestep may be summarized as follows

1. Calculate the fluid matrix $\mathcal{M}_n$ and the explicit term $\mathbf{b}^n$.
2. Solve for the updated pump configuration $\mathbf{X}^{n+1}$ via the matrix problem $(I + \sigma\mathcal{M}_n)\mathbf{X}^{n+1} = \sigma\mathbf{T}^{n+1} + \mathbf{b}^n$.
3. Calculate the updated fluid velocity $\mathbf{u}^{n+1}$ via the Stokes problem (9)-(10).
4. Calculate the updated polymeric stress $\mathbf{S}^{n+1}$ via the second-order TVD Runge-Kutta method, $\mathbf{S}^{n+1} = (\mathbf{S}^n + E(E(\mathbf{S}^n)))/2$.

4. Results

Here we summarize the results of our numerical simulations. We first present evidence to validate our methodology and then proceed to explore the extreme parameter regimes corresponding to very large wave amplitudes (occlusions) and very large Weissenberg numbers. We observe a new rich behavior which includes the potential formation of a finite time blow-up in the Oldroyd B model.

Two important values we will be observing are the flux and the normalized mean flow. We define the flux as

$$Q(x,t) = \int_{0.5-d(x,t)}^{0.5+d(x,t)} u(x,y)dy, \tag{20}$$

which is the total mass flux within the peristaltic pump across a specified vertical line. In this work we always take $x = 0.5$ and write $Q(t) = Q(x,t)$ for convenience. Closely related to the flux is the normalized mean flow, given by

$$\Theta(t) = \frac{\pi}{\alpha\chi}\int_t^{t+1} Q(t)dt. \tag{21}$$

Here we simply average and normalize the flux over one period of the peristaltic pump. The normalization leads to a dimensionless value, and is chosen such that $\Theta = 1$ when $\chi = 1$, regardless of the nature of the underlying fluid.

4.1. Resolution study and comparison to analytical results

We seek to validate our simulations through two approaches, by performing a spatial resolution study as well as by comparing simulations to known analytical results.

For the resolution study we consider the case when $\chi = 0.25$ and $We = 1$. We fix the time-step $\Delta t = 0.00025$ and run the simulation for a range of N from $N = 256$ up to $N = 2048$. We consider the $N = 2048$ run as our reference solution ("exact") and compute the errors of the other simulations in relation to this $N = 2048$ case. The results are given in Figure 1. In Figure 1(a) we examine the difference in flow Q at time $t = 1$. We observe less than a 1% relative error in Q for $N \geq 1024$. In Figure 1(b) we consider the sup norm of the difference of the xx-component of the stress. In both cases we observe slightly better than first order convergence, as expected from the convergence of the IB method.

There is a known analytic approximation of the mean flow Θ for the case of a Newtonian Stokes flow ($Re = 0$ and $We = 0$) due to Jaffrin and Shapiro [5]. The formula is given as

$$\Theta_J = \frac{15\chi^2 + 2\alpha^2[4(1-\chi^2)^{5/2} + (7\chi^2 - 4)(1-\chi^2)]}{\chi[5(2+\chi^2) + 6\alpha^2\chi^2(1-\chi^2)]} \tag{22}$$

In the Newtonian Stokes case Θ is a constant, thus the time of evaluation is not important so long as $T \geq 1$. In contrast our Navier-Stokes fluid has convection and takes a finite amount of time ($t < 1$) to reach a steady state. We take $t = 1$ and calculate Θ for a full range of χ, from 0 up to 0.95. We note that as $\chi \to 1$ the normal stresses on the walls of the pump become enormous. While the value $\sigma = 10^6$ is sufficient for $\chi = 0.95$, we note that for the case $\chi = 1$ even the extremely large value $\sigma = 10^8$ is insufficient to maintain the shape of the pump. In this extreme case the implicit methodology remains stable but the distortion of the geometry is great enough to warrant omitting the calculated mean flow.

The comparison of our simulated results, which have been checked under time and space refinement, to Jaffrin and Shapiro's formula can be seen in Figure 2. We see reasonably good agreement. We note, however, that for small to moderate occlusion ratios, the Stokes-OB results in [6] and our own results from explicit simulations provide slightly better agreement with the analytic formula. From our experience, we tend to believe that this small difference might be attributed to the somewhat better volume conservation

of the explicit method. Importantly, however, explicit simulations for the cases when $\chi \geqslant 0.5$ become impractical.

4.2. High occlusion, $\chi = .8$

Previous investigations utilizing the IB method to study peristaltic pumping have been limited to occlusions $\chi \leq 0.5$. With our implicit methodology we are able to explore for the first time occlusions in the range $0.5 < \chi < 1$ which induce extremely large polymeric stress forces on the peristaltic pump. Here we focus specifically on the case $\chi = 0.8$ and $We = 5$.

In Figures 9 through 12 we plot the polymeric stress evolution over time, for $N = 1024$ and $\Delta t = 0.00025$. We see first that the xx component of stress develops a strong concentration at the channel's neck, reaching a value of 360 at time $t = 0.5$. Soon after, at time $t = 1.5$, the xx-component is further concentrated into a nearly horizontal line, reaching a peak value of 18000. The two additional components $\mathbf{S}_{xy}$ and $\mathbf{S}_{yy}$ develop strong interfaces in identical locations, reaching values of 2400 and 6400 respectively. These strong interfaces effectively block off the inner interior of the peristaltic pump from any outside influences. This can be clearly seen in the vorticity plot, where the vorticity inside the interfaces is nearly zero. Outside the interfaces, near the boundary of peristaltic pump, we see strong, nearly uniform vorticity. As time progresses further, up to $t = 4.5$, we see the formation of more complex localized structures which again have strong effects on the vorticity. These fine structures eventually leads to instabilities and we are unable to reliably compute for longer than $t = 7$ for $N \geq 512$.

An important observation is that the strong thin line observed in the xx-component of the stress at time $t = 1.5$ dissipates over time and is significantly weaker at time $t = 4.5$. We suspect that this dissipation is due to numerical diffusion inherent to the ENO advection scheme. To investigate this further we perform a resolution study, focusing on the peak value of $\mathbf{S}_{xx}$ over the time interval $t = 0$ to $t = 1.5$.

First, in Figure 5(a) we plot $\mathbf{S}_{xx}$ over time for values of N ranging from $N = 256$ to $N = 2048$. We see that there is fast, nearly exponential growth, that levels off near $t = 1.5$. As N increases the maximum stress increases as well. We analyze the dependence on N in Figure 5(b). Here we plot $\|\mathbf{S}_{xx}\|_\infty$ at $t = 1.25$ versus $\log N$. We see that $\|\mathbf{S}_{xx}\|_\infty$ grows almost exactly proportional to $\log N$, yielding the approximate formula

$$\|\mathbf{S}_{xx}\|_\infty \approx 5286 \log N. \tag{23}$$

It is unclear if the relationship (23) persists for arbitrarily large N. If this were the case then it would be evidence for a finite time blow up in the

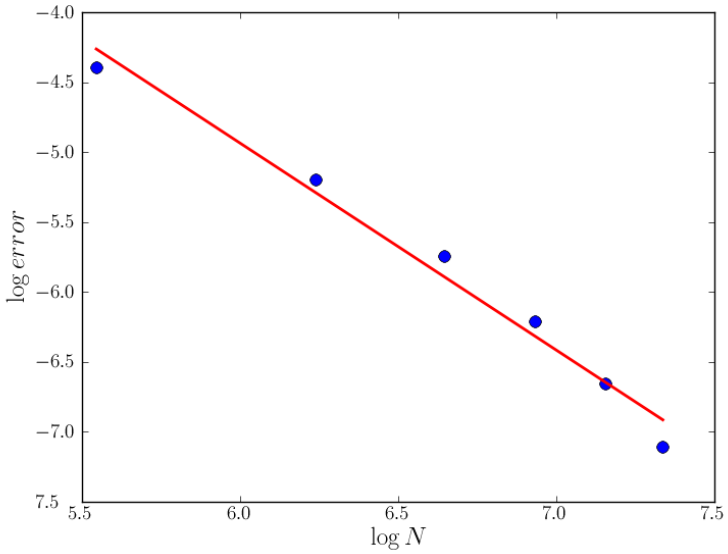

(a) Error of normalized flow $|Q - \tilde{Q}|$, $m = -1.479$.

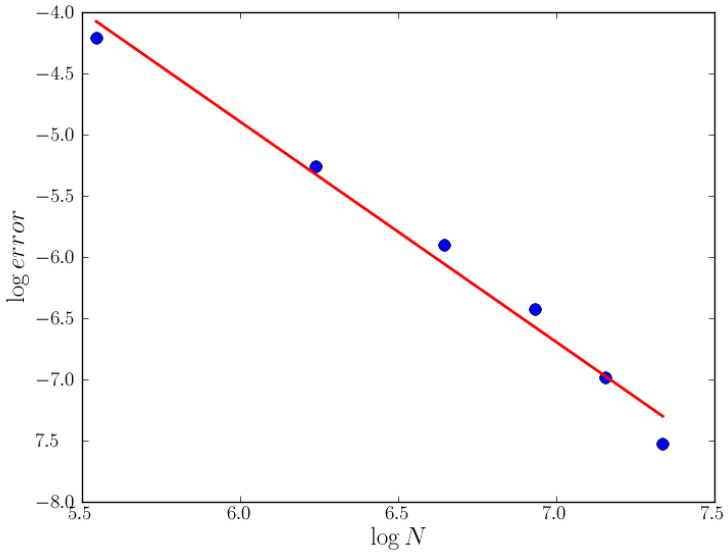

(b) Error of maximum stress $\left\|S_{xx} - \tilde{S}_{xx}\right\|_\infty$, $m = -1.800$.

Figure 1: Spatial resolution study for decreasing values of h. Value specified is plotted against h in a log-log plot. Variables with a tilde, $\tilde{\square}$, refer to values coming from an $N = 2048$ simulation taken to be an exact solution. Dashed lines are linear fits with specified slope m.

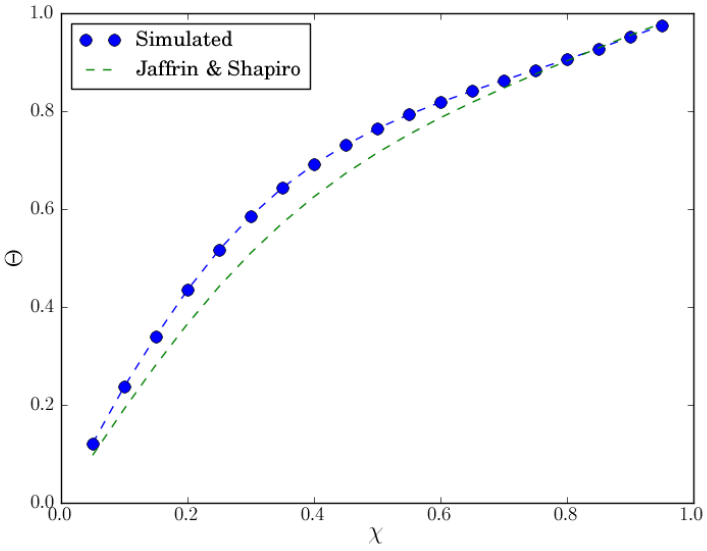

Figure 2: Normalized mean flow calculated both via Jaffrin and Shapiro's formula and numerical simulation for the full range of $\chi = 0$ to $\chi = 1$.

Oldroyd-B model for peristaltic pumping. To provide additional evidence we attempt to fit an exponential growth model of the form $C_N e^{\beta_N t}$ to the stress $\|\mathbf{S}_{xx}\|_\infty$ over the time interval $(0.36, 0.70)$. For $N = 2048$ the best fit is given by $C = 10, \beta = 7.68$. The fit is qualitatively good, as seen in Figure 6(a). We proceed to compute the best fit for various values of N and investigate the sequence $\{\beta_N\}$. In Figure 6(b) we plot β_N with respect to $\log N$ and notice a distinct linear trend. A linear fit yields $\beta_N \approx 0.3533 \log N$. We thus again see sharper growth as $N \to \infty$. This apparently unbounded behavior for the exponent points in the direction of a potential finite-time singularity in the polymeric stress.

The simulation for $\chi = 0.8$ is very challenging, involving very large stress and equally large restorative forces from the immersed structure. Very sharp interfaces develop in both the vorticity and stress. We present evidence that we are properly resolving these sharp interfaces. In Figure 3 we plot a simulation at time $t = 1.5$ for the case $\chi = 0.8, We = 5$. We compare the vorticity fields for both $N = 512$ and $N = 1024$ and note that the structure is qualitatively identical. Closer examination of the $N = 512$ plot reveals slightly blurred interfaces, indicative of the greater numerical diffusion at

lower resolutions. We observe similar results when we investigate the stress $\mathbf{S}$. We look at the Newtonian case in Figure 4 and note that the vorticity is well resolved. Indeed, we have observed that for the Newtonian case the vorticity is well resolved even for substantially lower resolutions, down to $N = 256$. The difference between the vorticity distributions of Newtonian and viscoelastic cases is striking.

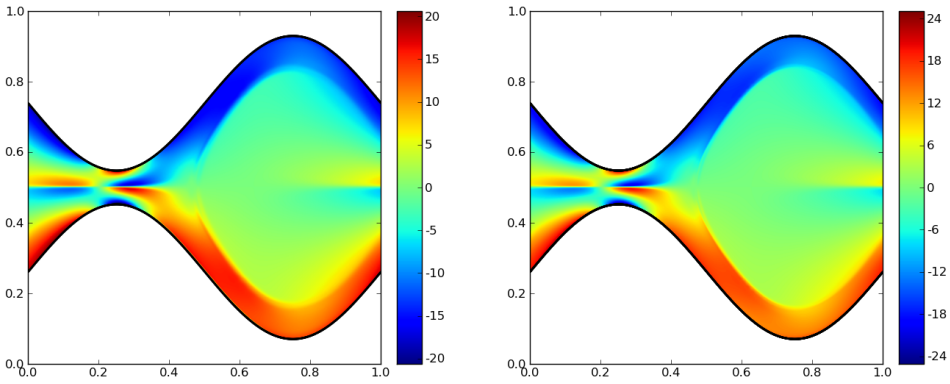

Figure 3: A comparison of the vorticity for a valve with $\chi = .8$ and $We = 5$ at time $t = 1.5$ for $N = 512$ and $N = 1024$ on the left and right respectively.

4.3. High Weissenberg number

Large values of We lead to large normal forces on the walls of the peristaltic pump. These forces in turn require large stiffness constants σ to properly maintain the prescribed shape of the walls. Previous investigations by Teran, Fauci and Shelley [6] and Chrispell and Fauci [3] were limited to Weissenberg numbers $We \leq 5$. With our superior methodology we are able to investigate for the first time higher Weissenberg numbers, up to and beyond $We = 100$.

We investigate first the case $We = 55$, $\chi = 0.5$. In Figures 13 through 16 we plot the polymeric stress evolution over time, for $N = 1024$ and $dt = .00025$. We note first that all components of the stress $\mathbf{S}_{xx}, \mathbf{S}_{xy}, \mathbf{S}_{yy}$ develop multilayered interfaces by time $t = 8.4$. As time progresses, however, these interfaces merge into smooth, simple regions. By time $t = 18.9$ no indication is left of the intricate, multilayered interfaces. We suspect that this smoothing is due to the numerical diffusion inherent to the ENO convection scheme.

An interesting question is how the normalized mean flow Θ responds to changes in We and χ. In Figure 7 we plot Θ at time $t = 15$ (Figure 7(a)) and $t = 50$ (Figure 7(b)) for $We = 0$ up to $We = 105$, and for $\chi = 0$ up to $\chi = 0.75$. We note a modest effect of the Weissenberg number on Θ, with higher values of We corresponding to higher mean flows. The dependence of Θ on t is more complicated. For $We \leq 5$ it appears that a semi-steady state

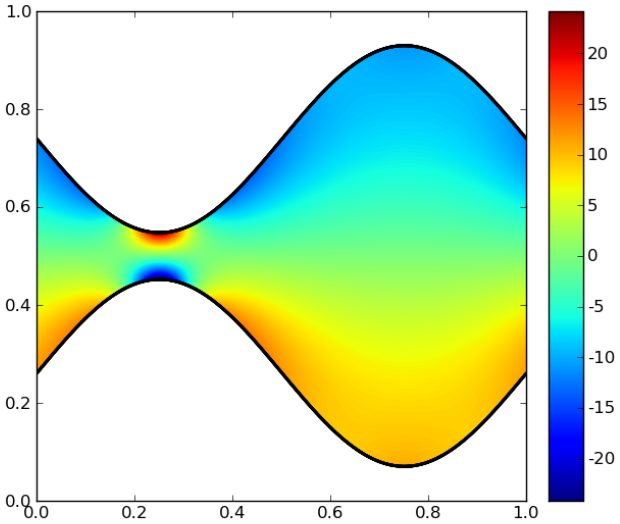

Figure 4: Vorticity for a valve with occlusion $\chi = .8$ in a Newtonian flow at time $t = 1.5$.

is eventually reached. The time required to reach this semi-steady state was given to be $3We$ in [6, 3], and we see a similar requirement for the regimes studied in [6, 3].

For higher We we report substantially different behavior. We examine the mean flow over time in Figure 8. For $\chi = 0.4$ and $We = 5$, displayed in Figure 8(a), we see relatively little variation in mean flow over time, consistent with previous results. For $We \geq 25$, however, we see substantially more complex behavior. For $We = 25$ the mean flow appears to become reasonably consistent after $t = 70$, despite large variations. For $We = 55$ and $We = 105$ no semi-steady state is reached for our simulation times ($T < 150$). For $\chi = 0.6$ we see long term variation in the mean flow even for the small value of $We = 5$. The flow appears to reach and maintain a semi-steady state for a long duration of time, from $t = 20$ to $t = 70$ (50 periods of the pump), but then has a sudden drop in mean flow at time $t = 70$.

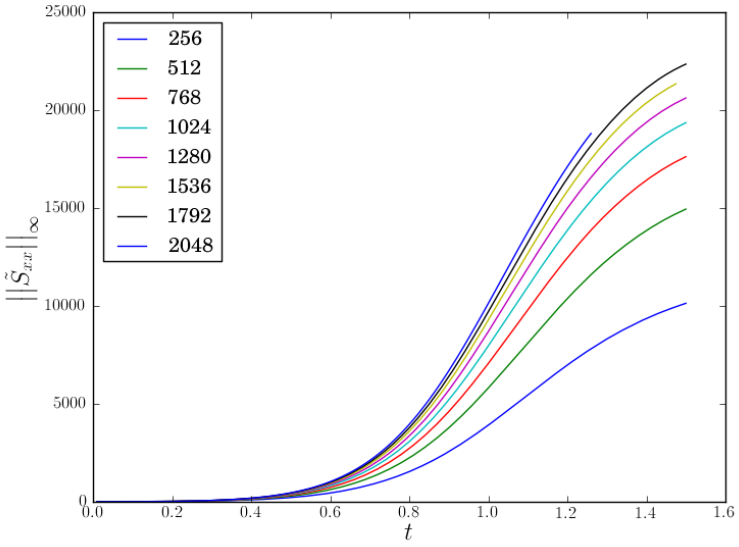

(a) $\left\|\bar{S}_{xx}(t)\right\|_\infty$ over the time interval $(0, 1.5)$ for various values of N.

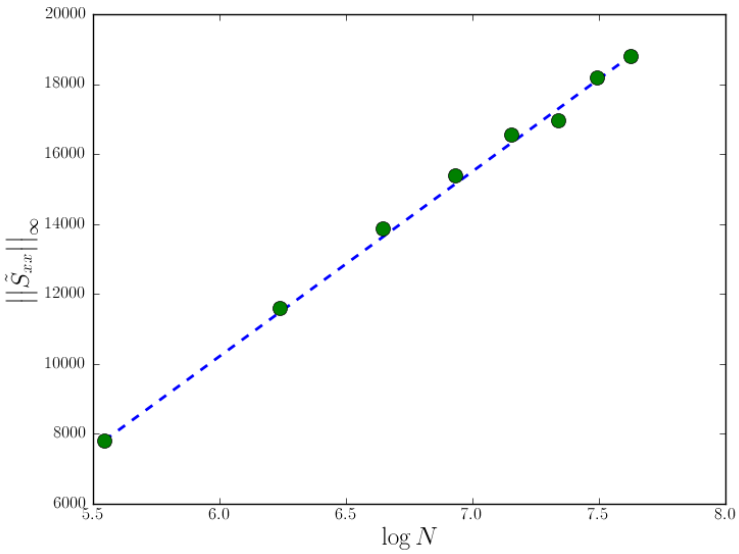

(b) $\left\|\bar{S}_{xx}(t)\right\|_\infty$ at time $t = 1.25$, plotted against $-\log h$, as N varies from 256 to 2048. Dashed line is a linear fit with slope $m = 5286$

Figure 5: Resolution study of the sup norm of the stress component S_{xx} along the horizontal line of symmetry, denoted as $\left\|\bar{S}_{xx}(t)\right\|_\infty$ at time t.

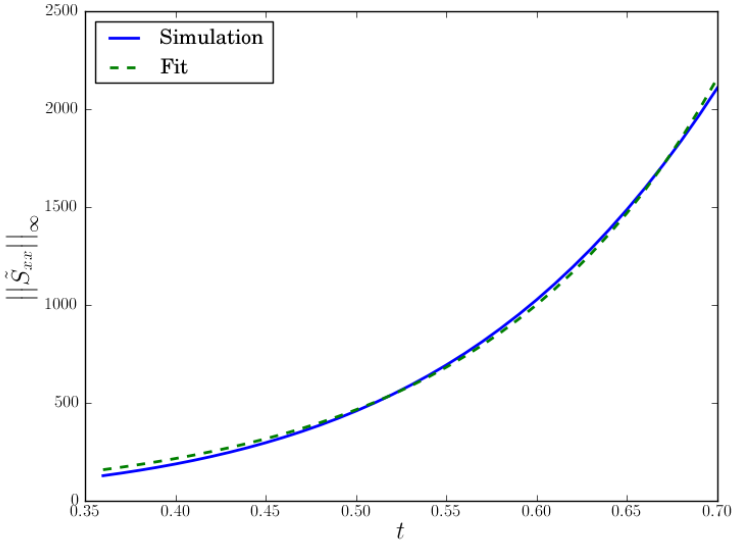

(a) $\left\|\bar{S}_{xx}(t)\right\|_\infty$ over the time interval $(0.36, 0.70)$ for $N = 2048$. Matched fit is the exponential curve $10e^{7.68t}$.

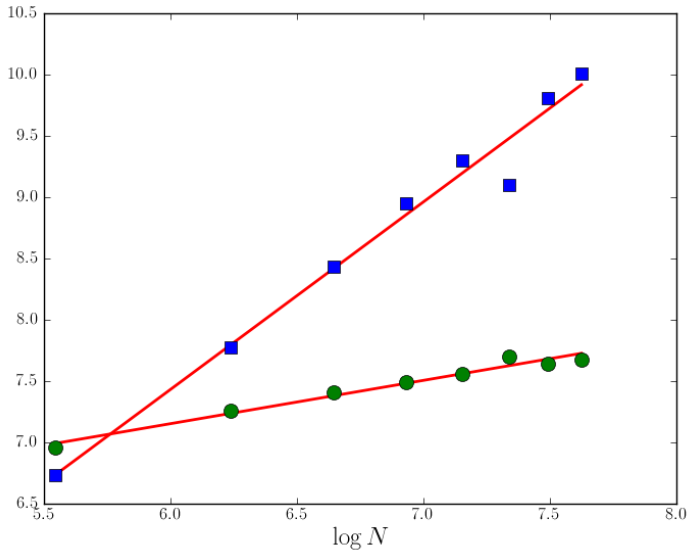

(b) β_N ($\circ$) and C_N ($\square$) with respect to $\log N$. The solid line is a linear fit with slope $m = 0.3533$

Figure 6: Consider $\left\|\bar{S}_{xx}(t)\right\|_\infty$ over the timer interval $(0.36, 0.70)$ for a specified resolution N. We compute a best fit of the form $C_N e^{\beta_N t}$, in the L^2 sense.

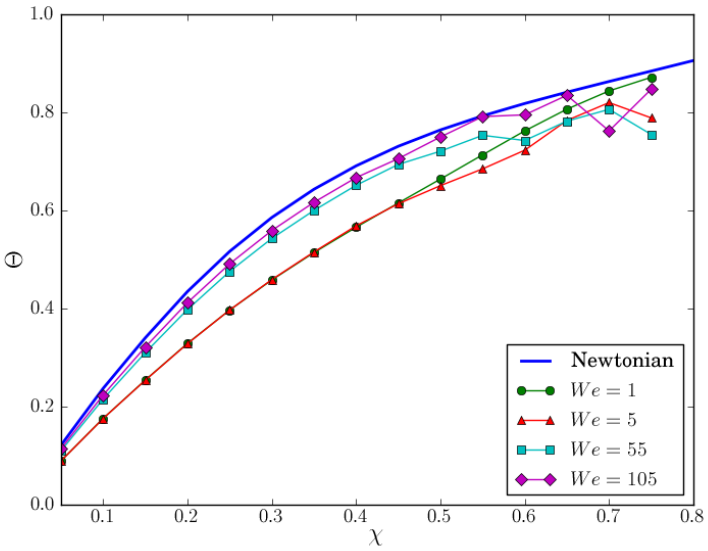

(a) Normalized mean flow at time $t = 15$ for various values of We and χ.

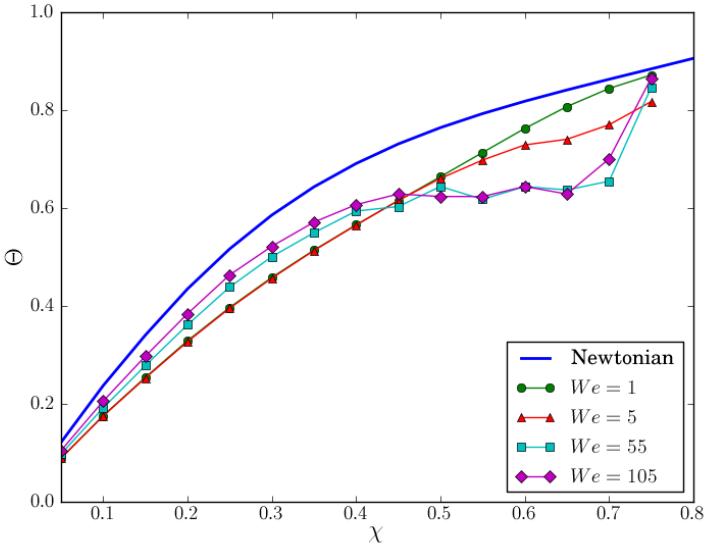

(b) Normalized mean flow at time $t = 50$ for various values of We and χ.

Figure 7: Normalized mean flow at times $t = 15$ and $t = 50$ for various values of We and χ.

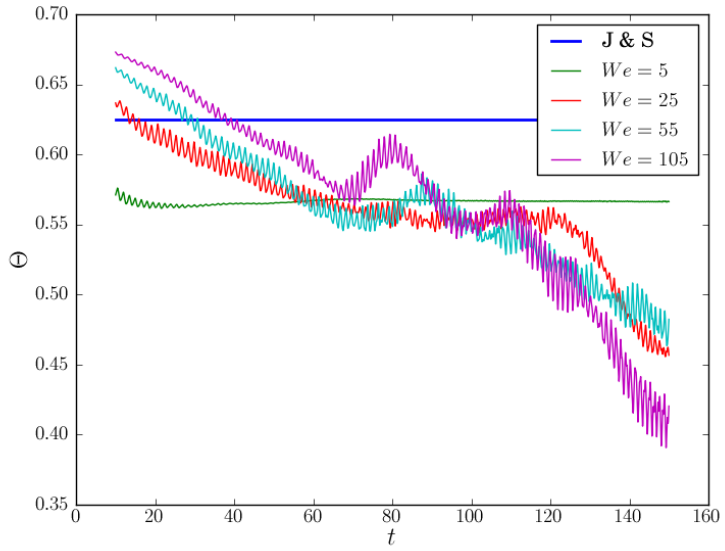

(a) $\chi = 0.4$

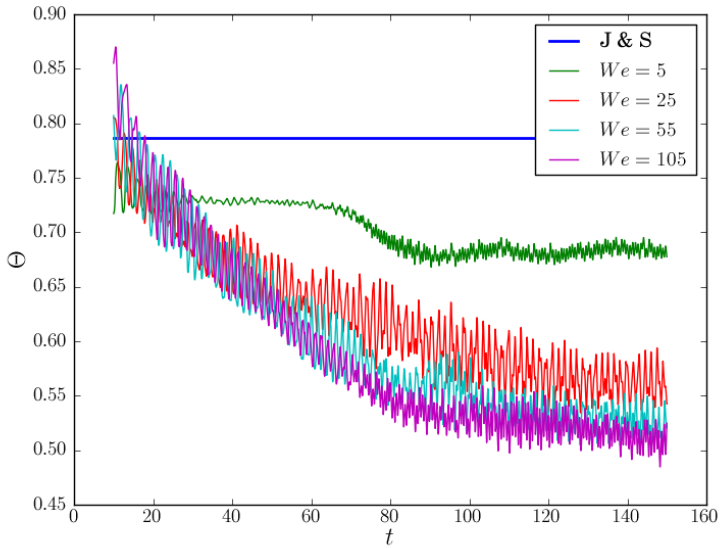

(b) $\chi = 0.6$

Figure 8: Mean flow Θ over time for various values of We. Top and bottom plot are for $\chi = 0.4$ and $\chi = 0.6$ respectively.

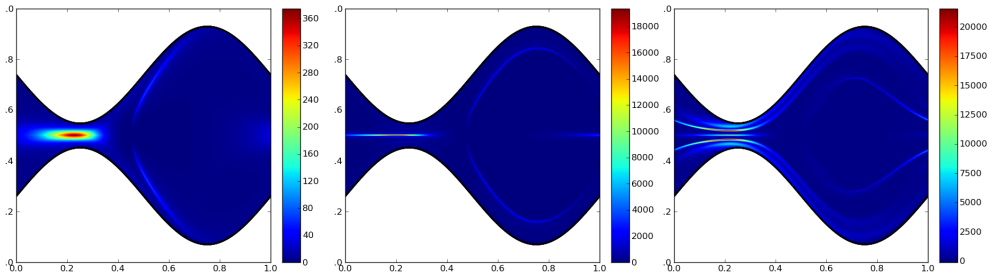

Figure 9: S_{xx} at times $t = .5$, $t = 1.5$, $t = 4.5$.

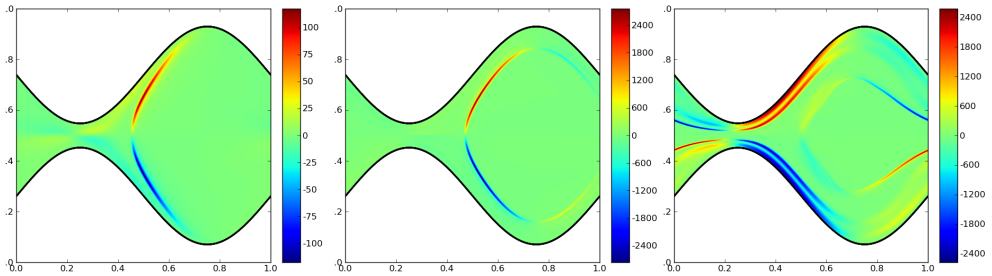

Figure 10: S_{xy} at times $t = .5$, $t = 1.5$, $t = 4.5$.

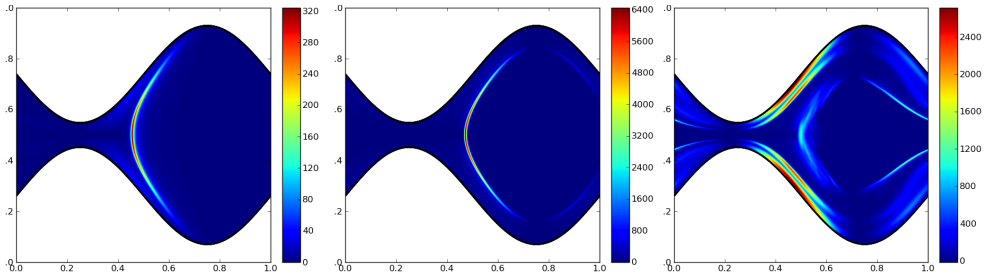

Figure 11: S_{yy} at times $t = .5$, $t = 1.5$, $t = 4.5$.

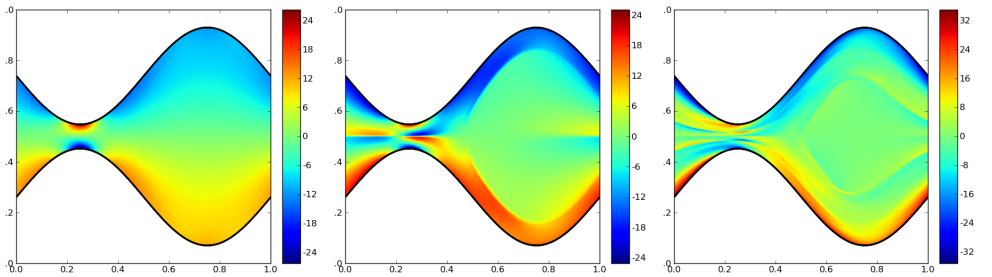

Figure 12: Vorticity of the fluid velocity at times $t = .5$, $t = 1.5$, $t = 4.5$.

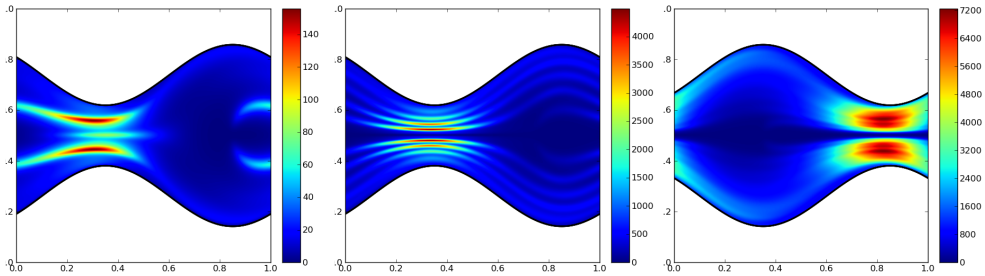

Figure 13: S_{xx} at times $t = 1.4$, $t = 8.4$, $t = 18.9$.

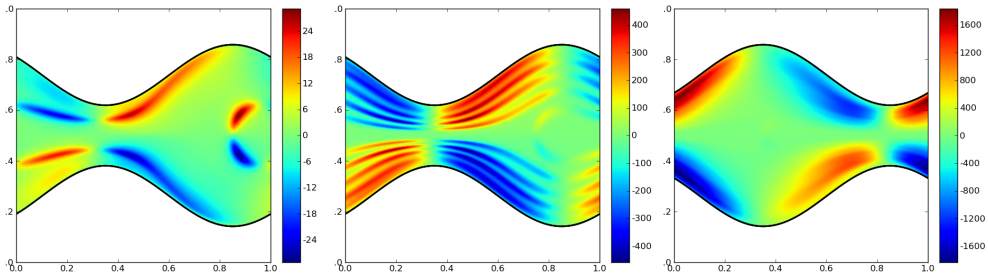

Figure 14: S_{xy} at times $t = 1.4$, $t = 8.4$, $t = 18.9$.

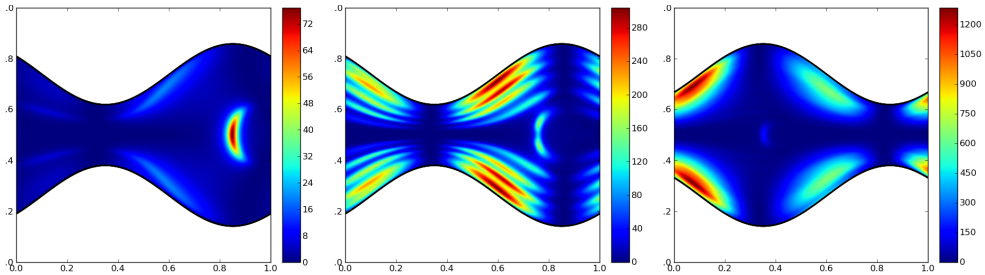

Figure 15: S_{yy} at times $t = 1.4$, $t = 8.4$, $t = 18.9$.

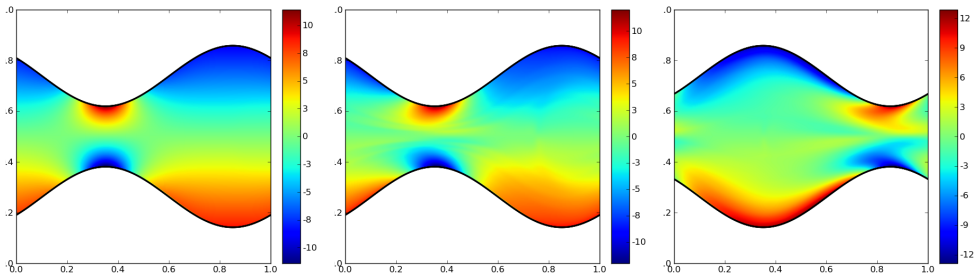

Figure 16: Vorticity of the fluid velocity at times $t = 1.4$, $t = 8.4$, $t = 18.9$.

5. Conclusion

Previous investigations into peristaltic pumping of OB fluids have revealed that the gross transport properties of the pump are highly sensitive to the underlying fluid parameters. Making use of a new implicit methodology we are able to explore a much broader parameter regime, observing new behavior both for high occlusion ratios and high Weissenberg numbers.

Future work will focus on extending this investigation to three dimensions, where preliminary results suggest new and different behavior. Importantly, in 3D we can investigate a plethora of novel asymmetrical pump geometries, including cork-screw like shapes. Preliminary results also suggest interesting differences when the OB fluid is replaced with a FENE-P fluid. Future work will explore these differences.

Acknowledgments

The authors would like to thank John Chrispell for his helpful advice on the Oldroyd-B model as it pertains to peristaltic pumping. Computations were performed on the Knot cluster at the California NanoSystems Institute Computing Facility, funded by the National Science Foundation under grant CNS-0960316. Special thanks to Fuzzy Rogers and Paul Weakliem at CNSI for their help working with the cluster. Partial support for this work was provided by the National Science Foundation under grant DMS-1016310.

References

[1] H. D. Ceniceros, J. E. Fisher, and A. M. Roma. Efficient solutions to robust, semi-implicit discretizations of the immersed boundary method. *Journal of Computational Physics*, 228(19):7137 – 7158, 2009.

[2] H.D. Ceniceros and J.E. Fisher. A fast, robust, and non-stiff immersed boundary method. *Journal of Computational Physics*, 2011.

[3] J. Chrispell and L. Fauci. Peristaltic pumping of solid particles immersed in a viscoelastic fluid. *Bulletin of the American Physical Society*, 55, 2010.

[4] B.E. Griffith. On the volume conservation of the immersed boundary method. *Submitted, preprint available from http://www. cims. nyu. edu/ griffith.*

[5] MY Jaffrin and AH Shapiro. Peristaltic pumping. *Annual Review of Fluid Mechanics*, 3(1):13–37, 1971.

[6] J. Teran, L. Fauci, and M. Shelley. Peristaltic pumping and irreversibility of a stokesian viscoelastic fluid. *Physics of Fluids*, 20:073101, 2008.